Phys. Med. Biol. **45** (2000) 1553–1563. Printed in the UK PII: S0031-9155(00)07002-0

Precision estimation and imaging of normal and shear components of the 3D strain tensor in elastography

Elisa E Konofagou and Jonathan Ophir

Ultrasonics Laboratory, Department of Radiology, The University of Texas Medical School, Houston, TX 77030, USA

Received 16 August 1999, in final form 8 November 1999

Abstract. In elastography we have previously developed a tracking and correction method that estimates the axial and lateral strain components along and perpendicular to the compressor/scanning axis following an externally applied compression. However, the resulting motion is a three-dimensional problem. Therefore, in order to fully describe this motion we need to consider a 3D model and estimate all three principal strain components, i.e. axial, lateral and elevational (out-of-plane), for a full 3D tensor description.

Since motion is coupled in all three dimensions, the three motion components have to be decoupled prior to their estimation. In this paper, we describe a method that estimates and corrects motion in three dimensions, which is an extension of the 2D motion tracking and correction method discussed before. In a similar way as in the 2D motion estimation, and by assuming that ultrasonic frames are available in more than one parallel elevational plane, we used methods of interpolation and cross-correlation between elevationally displaced RF echo segments to estimate the elevational displacement and strain. In addition, the axial, lateral and elevational displacements were used to estimate all three shear strain components that, together with the normal strain estimates, fully describe the full 3D normal strain tensor resulting from the uniform compression. Results of this method from three-dimensional finite-element simulations are shown.

(Some figures in this article appear in colour only in the electronic version; see `www.iop.org`)

1. Introduction

Elastography is an imaging modality that provides insight into the elastic properties of biological tissues by applying a small axial uniform compression, and imaging the resulting local strains (Ophir *et al* 1991, Céspedes 1993, Garra *et al* 1997). Until recently, only the axial strain component had been estimated and used to produce a strain image, the axial elastogram. However, motion in tissues occurs in three dimensions which involves inevitable coupling between the three main strain components. Therefore, estimation of motion in the other two directions is imperative in order to provide important information on the mechanical properties of tissues (Konofagou and Ophir 1998), such as anisotropy, compressibility, poroelasticity (Konofagou *et al* 1999) and/or viscoelasticity, as well as correction for decorrelation in the axial strain estimation (Chaturvedi *et al* 1998, Insana *et al* 1997, Konofagou and Ophir 1998). Signal decorrelation, caused by the relative motion of tissue scatterers following the compression, is the primary cause for the increase in the strain estimation variance (Kallel *et al* 1997). Konofagou and Ophir (1998) recently discussed simultaneous estimation of both axial and lateral motions using a precision tracking and recorrelation method. In this paper we apply the same method in all three dimensions in order to estimate all three normal strain components, i.e. axial, lateral and elevational (out-of-plane) components. The principle of the tracking

0031-9155/00/061553+11$30.00

and recorrelation method is that by decoupling the estimated motion components, the signals used for motion estimation are recorrelated and the signal-to-noise ratio associated with the estimation of each motion component is significantly increased (Konofagou and Ophir 1998).

Two distinct estimators for tracking elevational motion can be developed using (a) a single plane or (b) multiple planes. When only one plane is available, motion in the elevational direction can be tracked by using the decorrelation information (Li *et al* 1999). Bamber and Bush (1996) also used the correlation coefficient of the signal envelope to generate lateral displacement images. However, Alam and Ophir (1997) demonstrated that, in the axial case, changes in the centre frequency and sonographic signal-to-noise ratio (SNR_s) introduce unknown variable bias errors. Therefore, this method was not considered. In the case where multiple (1.5D or 2D) arrays are used (figure 1), an interplanar tracking method, similar to the one used for interbeam lateral tracking (Konofagou and Ophir 1998), may be applied in the elevational direction.

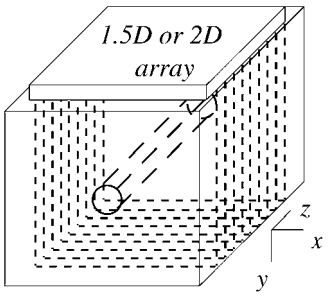

Figure 1. Simulation of a 3D phantom containing a cylindrical inclusion and scanned by a 1.5D or 2D array. The phantom was uniformly compressed in the y- (axial) direction while the x- and z-directions denote the lateral and elevational directions, respectively. The dotted lines represent the parallel scanning planes in the z-direction.

In axial motion estimation, decorrelation noise is introduced by motion in the lateral and elevational directions (Kallel and Ophir 1997). In a similar way, when *elevational* strain is estimated, decorrelation noise due to undesired motion in the axial and/or lateral direction is expected to corrupt the estimate, with the axial motion being the most important due to loss of phase coherence (both the applied compression and ultrasonic scanning are in the axial direction). Other sources of decorrelation, such as rotation and shear strain, were not considered. A method that interchangeably estimates *and* corrects for motion in the axial, lateral and elevational directions was developed (figure 2). A two-dimensional version of this method was used by Konofagou and Ophir (1998) to correct the axial elastogram for lateral decorrelation. The method decouples the three main strain components, and thereby estimates and images all three orthogonal displacement components (u_x, u_y and u_z) that can be used to estimate the normal (ε_x, ε_y, ε_z) as well as shear (ε_{xy}, ε_{yz} and ε_{xz}) strain components that fully characterize the 3D normal strain tensor given by

$$E = \begin{bmatrix} \varepsilon_x & \varepsilon_{xy} & \varepsilon_{xz} \\ \varepsilon_{yx} & \varepsilon_y & \varepsilon_{yz} \\ \varepsilon_{zx} & \varepsilon_{zy} & \varepsilon_z \end{bmatrix} \tag{1}$$

where

$$\varepsilon_{ij} = \frac{1}{2}\left(\frac{\partial u_i}{\partial X_j} + \frac{\partial u_j}{\partial X_i}\right) \tag{2}$$

and X denotes the coordinate in the lateral (x-), axial (y-) and elevational (z-) directions.

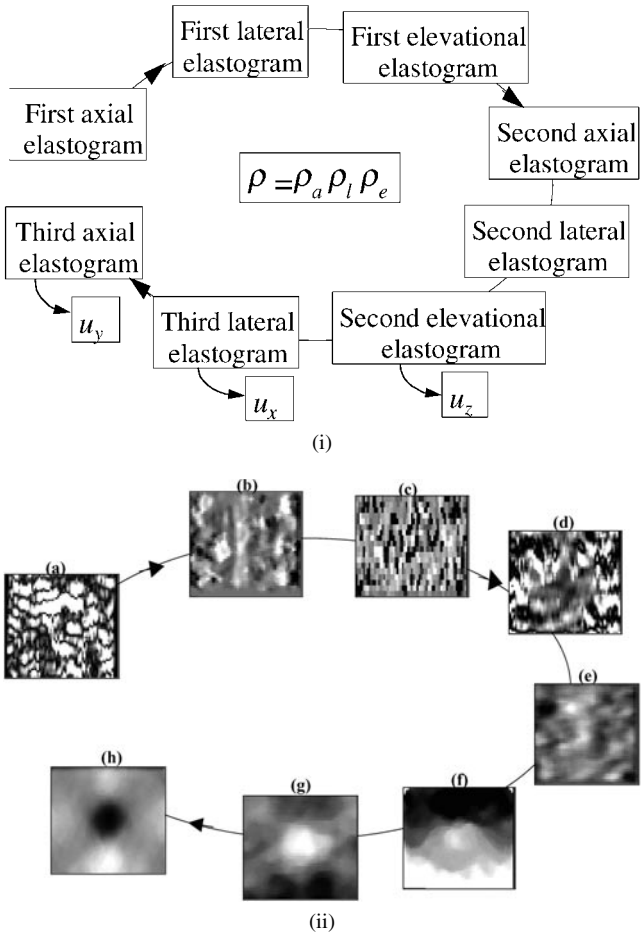

Figure 2. (i) 3D recorrelation method of displacement and strain (elastogram) estimation and correction and (ii) all elastograms follow the same order as (i), i.e. (*a*) first axial, (*b*) first lateral, (*c*) first elevational, (*d*) second axial, (*e*) second lateral, (*f*) second elevational, (*g*) third lateral, (*h*) third axial elastograms. The true axial, lateral and elevational strain images are shown in figures 4(*a*), (*b*) and (*c*) respectively. Positive and negative strain values denote compressive and tensile strains respectively.

There are three distinct ways in which multiple planes can be generated in the elevational direction. Firstly, this may be done by displacing a 1D linear array in the elevational direction and acquiring successive frames at different parallel elevational planes. This method will most probably not be workable in an experimental setting since the compression in each scanning plane would involve different boundary conditions and thereby different motion fields, rendering elevational tracking most difficult. Secondly, a 1.5D array can be used to provide three to four elevational planes by firing different sets of elements in the elevational direction. This method may yield the elevational component. Lastly, a 2D (or $N \times N$) array may be used, providing as many planes in the elevational direction as there are beams in the lateral direction. In this case, elevational motion can be estimated in a plane perpendicular to a certain scanning plane. In all cases, an interplanar tracking approach can be applied, similar to the lateral tracking method. In this paper, we simulated both 1.5D and 2D arrays, as described below (figure 1).

2. Theory

A three-dimensional point spread function (psf)

$$p(x, y, z) = p_a(y)p_l(x)p_e(z) \tag{3}$$

was simulated, where x, y and z are the axial, lateral and elevational coordinates respectively and $p_a(y)$, $p_l(x)$ and $p_e(z)$ are the axial, lateral and elevational psf components respectively. If we assume a Gaussian modulated emitted pulse of pulse length equal to σ_y, the axial psf component is given by

$$p_a(y) = A \exp\left(-\frac{y^2}{2\sigma_y^2}\right) \cos\left(2\pi \frac{y}{\lambda}\right) \tag{4}$$

where A is a constant and λ is the central wavelength of the emitted pulse. The lateral and elevational psf components may be modelled as Gaussian functions (Wagner *et al* 1983), and are respectively given by

$$p_l(x) = \frac{1}{\sqrt{2\pi}\sigma_x} \exp\left(-\frac{x^2}{4\sigma_x^2}\right) \tag{5}$$

and

$$p_e(z) = \frac{1}{\sqrt{2\pi}\sigma_z} \exp\left(-\frac{z^2}{4\sigma_z^2}\right) \tag{6}$$

where σ_x and σ_z are the lateral and elevational correlation lengths respectively. In order to simulate the pre- and postcompressed 3D RF sonograms, we followed a previously described convolutional model. The pre- and post-compression echo signals can respectively be given as follows†:

$$r_1(x, y, z) = p(x, y, z) * e(x, y, z) + n_1(x, y, z) \tag{7}$$

$$r_2(x, y, z) = p(x, y, z) * e(a_1x - x_0, a_2y - y_0, a_3z - z_0) + n_2(x, y, z) \tag{8}$$

where $*$ denotes convolution, x_0, y_0 and z_0 correspond to the lateral, axial and elevational delays or displacements, $r_1(x, y, z)$ and $r_2(x, y, z)$ are the received RF signals before and after compression respectively, $p(x, y, z)$ is the PSF, $e(x, y, z)$ is the scattering function, $n_1(x, y, z)$ and $n_2(x, y, z)$ are independent zero-mean white noise sources and a_1, a_2 and a_3 are the scaling coefficients due to lateral, axial and elevational strains respectively.

The correlation coefficient for one-dimensional motion (axial, lateral or elevational) estimation, or time delay estimation (TDE), is typically defined by Bendat and Piersol (1986) as

$$\rho_{12}(\tau) = \frac{R_{12}(\tau)}{\sqrt{R_{11}(0)R_{22}(0)}} \tag{9}$$

where τ is the delay (equal to the displacement in elastography) and $R_{12}(\tau)$ is the peak of the cross-correlation function given by

$$R_{12}(\tau) = \frac{1}{T}\int_0^T r_1(t)r_2(t + \tau)\,\mathrm{d}t \tag{10}$$

where $r_1(t)$ and $r_2(t)$ are the received RF signals before and after compression respectively, T is the window length and t denotes a time or spatial variable. Meunier (1989) calculated the

† In the axial direction, distance is proportional to time, since the speed of sound in the tissue is assumed constant and equal to 1540 m s^{-1}. Therefore, spatial variables (such as displacement) are proportional to time variables (such as time delay) and vice versa.

theoretical expression for the axial correlation coefficient (assuming infinite window size), ρ_a, and found it to be equal to

$$\rho_a = 2\sqrt{\frac{\alpha\beta}{(\alpha^2+1)(\beta^2+1)}}\exp\left[-\frac{1}{2}\left(\frac{(\alpha^2-1)^2 f_0^2}{2\sigma_y^2(\alpha^2+1)}\right)\right] \tag{11}$$

where

$$\alpha = \frac{1}{1-\varepsilon_a} \approx 1+\varepsilon_a \tag{12}$$

and where α is the compression factor as a function of the uniformly applied axial strain ε_a, and β is the lateral expansion factor. In a similar fashion, Kallel and Ophir (1997) derived the expressions for the lateral and elevational correlation coefficients given respectively by

$$\rho_l \approx \exp\left(-k\frac{(-\nu\varepsilon_a x_0)^2}{\sigma_x^2}\right) \tag{13}$$

and

$$\rho_e \approx \exp\left(-k\frac{(-\nu\varepsilon_a z_0)^2}{\sigma_z^2}\right) \tag{14}$$

where k is a constant (equal to 1.2), ν is Poisson's ratio and x_0 and z_0 are the lateral and elevational tissue displacements from the axes of symmetry in the respective directions. Kallel and Ophir (1997) also derived the expression for the effective correlation coefficient ρ associated with 3D motion to be

$$\rho = \rho_a\rho_l\rho_e \tag{15}$$

under the assumption that the three psf components (equations (4)–(6)) are separable. The effective correlation coefficient ρ determines the amount of decorrelation noise in each elastogram and depends on *all* (i.e. axial, lateral and elevational) motion components (Kallel and Ophir 1997): the higher the correlation coefficient, the higher the signal-to-noise ratio in the axial, lateral and elevational motion estimation. According to equations (11), (13), (14) and (15), the highest correlation coefficient is achieved when the compression factor is closest to 1 and the lateral and elevational displacements are zero, or, in a 3D setting, are estimated and corrected for. The recorrelation method achieves an increase of each correlation coefficient through successive use of axial global stretching, lateral tracking and correction and elevational tracking and correction.

3. Methods

The axial psf component had a 50% bandwidth and a 5 MHz centre frequency while the lateral and elevational psf components had full widths at half-maximum (FWHM $\approx 2.35\sqrt{2}\sigma_x = 2.35\sqrt{2}\sigma_z$), or beamwidths, of 2 mm. The number of A-lines in the lateral direction was always 60, while in the elevational direction, 4 and 60 beams were respectively used in the cases of the 1.5D and 2D arrays. Both the lateral and elevational pitches were equal to 0.67 mm. A 3D incompressible phantom of $40 \times 40 \times 20$ mm^3 containing a 10 mm diameter cylindrical inclusion (of length equal to the girth of the phantom, i.e. 20 mm) was built with the finite-element analysis (FEA) software ALGOR† (figures 1 and 3). The inclusion was three times stiffer than the background (stiffness of 21 kPa) and both inclusion and background were incompressible, i.e. with a Poisson's ratio of 0.5. The 3D phantom was compressed from

† ALGOR is a registered trademark of Algor, Inc.

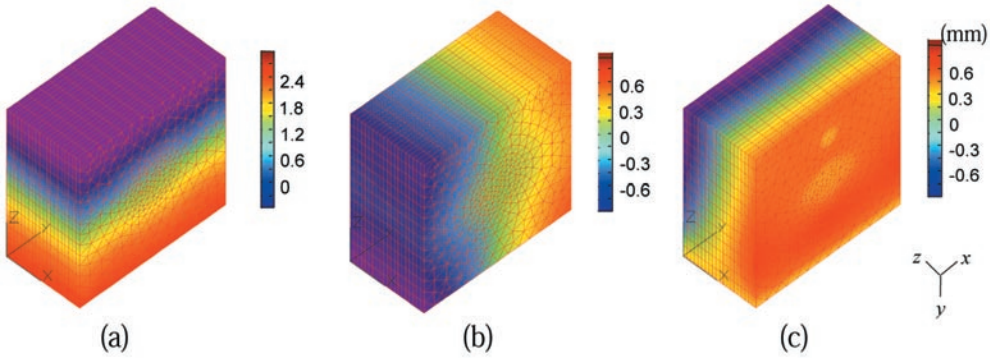

Figure 3. 3D representation of finite-element calculated (*a*) axial, (*b*) lateral and (*c*) elevational displacement images of the 3D ALGOR phantom.

the top (along the *y*- or axial direction, figure 1), fixed at the bottom, with slip and non-slip conditions in the *x*- (lateral) and *z*- (elevational) directions respectively. The non-slip conditions in at least one dimension were imperative in the 3D case, otherwise the phantom would have unstable conditions under compression. All lateral sides were free. The 3D RF sonograms were obtained in MATLAB‡ through convolution of the psf of equation (3) with a tissue scattering function as shown in Konofagou and Ophir (1998). The scatterers moved according to the FEA displacement solution. Monte Carlo simulations in MATLAB were used to generate pre- and postcompression RF signals. The scattering function consisted of uniformly distributed point scatterers with a density of 40 scatterers/pulsewidth, whose amplitudes followed Gaussian statistics. We assume that the uniformly distributed scatterers were of a sufficient number to generate an echo signal with Gaussian statistics (Insana *et al* 1986, 1990). The PSF was convolved with the scattering function to obtain the precompression RF signal following equation (7). The postcompression signals were generated after applying a uniform compression to the point scatterers (Céspedes 1993), and convolving the compressed point scatterers with the original PSF following equation (8).

In order to highlight the importance of the correction, we considered an example with high decorrelation noise. The method, due to its precision, can correct for smaller decorrelation as well (Konofagou and Ophir 1998). We considered the case of 6% applied strain (equivalent to 2.4 mm applied displacement) and scanned in a plane at the elevational edge of the phantom, i.e. away from the elevational plane of symmetry, where the motion in the elevational direction was the largest, and therefore decorrelation noise was maximized. In order to estimate motion in all three directions, a 3D recorrelation method was applied.

First, the strain components were estimated without correction producing the *first* axial, lateral and elevational elastograms. Axial strain was determined using the seven-point least-squares estimator (Kallel and Ophir 1997) on axial displacement estimates, which were determined using the standard method of cross-correlation of pre- and postcompressed RF segments (Ophir *et al* 1991). The window size was 3 mm and the window overlap 80%. The lateral (or elevational) displacement was computed by interpolating between original postcompressed A-lines and cross-correlating pre- and postcompressed RF segments in the lateral (or elevational) direction (Konofagou *et al* 1998). The lateral (or elevational) strain was then estimated using the least-squares estimator with a kernel of 10 points. At each subsequent step of the recorrelation method (figure 2(i)) a new postcompression RF sonogram

‡ MATLAB (Version 5.2) is a registered trademark of Mathworks, Inc, Natick, MA, USA.

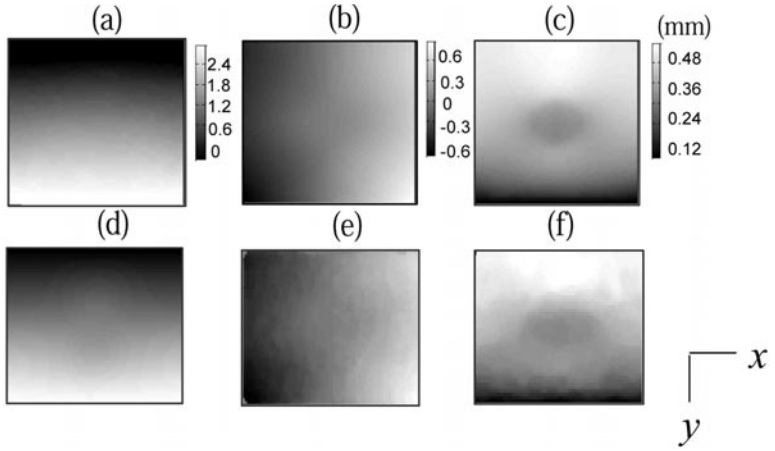

Figure 4. True (*a*) axial (u_y), (*b*) lateral (u_x) and (*c*) elevational (u_z) and estimated (*d*) axial, (*e*) lateral and (*f*) elevational displacement images (in mm), all estimated in the same plane at the elevational edge of the phantom (figure 3).

was produced that had been corrected for the motion estimated at that step and was to be used in the following step. The *second* axial and lateral elastograms were corrected for axial decorrelation through the use of global stretching (Varghese *et al* 1996) and the same method of cross-correlation estimation, as described above, was applied. The second lateral elastograms were generated by applying the gradient operator to the lateral displacements, estimated using linear interpolation and tracking of axial *single* RF segments (Konofagou and Ophir 1998). The second elevational elastogram was calculated using the stretched and laterally shifted RF segments (Konofagou and Ophir 1998). The lateral displacement used to generate the second lateral elastogram was used for laterally shifting the RF segments prior to estimation of the second elevational elastogram. Finally, the *third* axial and lateral elastograms were calculated following elevational correction by shifting the RF segments in the elevational direction by the amount of estimated elevational displacement. The linear interpolation scheme in both lateral and elevational estimation was 50:1. The recorrelation method was applied in two simulated cases, using (a) a 1.5D array (60×4 A-lines) where all axial, lateral and elevational motions were estimated with respect to the same axial plane (at the elevational edge of the target), and (b) a 2D array (60×60 A-lines), where elevational motion was estimated in a plane perpendicular to the axial plane and along the axis of the cylindrical inclusion.

4. Results

4.1. 1.5D array example

All *first axial, first lateral* and *first elevational* elastograms are estimated at 6% axial compression. The outcomes (figures 2(ii)(*a*), (*b*) and (*c*)) are severely corrupted by decorrelation noise, as expected. The correction starts with global stretching (Varghese *et al* 1996) that removes the decorrelation noise due to axial motion. This step yields the *second axial* and *second lateral* elastograms (figures 2(ii)(*d*) and (*e*)). The lateral displacement measured in the second lateral step is used for lateral correction by using the same correction method as described in the previous section. The *second elevational* displacement image (figure 4(*f*)) and elastogram (figures 2(ii)(*f*) and 5(*f*)) are generated using the postcompression data corrected

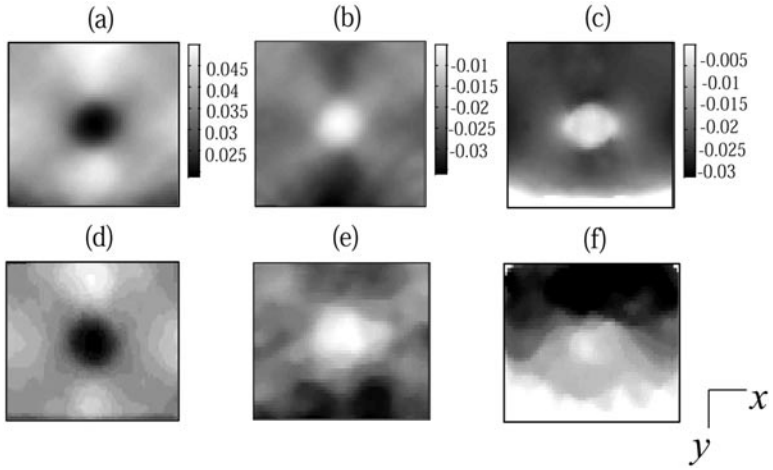

Figure 5. Elastograms of ε_y, ε_x and ε_z normal strain components corresponding to the displacement images of figure 4. Positive and negative strain values denote compressive and tensile strains respectively.

for axial and lateral motion. The elevational displacement image describes motion in the elevational direction in and out of the 2D outer plane that is the front face of figure 3(*c*). Motion in the elevational direction is only positive because all motion in that particular plane has occurred in the positive elevational direction (figure 4(*f*)).

The third *lateral* displacement image (figure 4(*e*)) and elastogram (figures 2(ii)(*g*) and 5(*e*)) are generated after correction for elevational motion and the *third axial* displacement (figure 4(*d*)) and strain (figures 2(ii)(*h*) and 5(*d*)) images, which have been corrected for elevational and lateral motion. Throughout this recorrelation method, the signal-to-noise ratio (SNR_e) of all three elastograms rises steadily, since the effective correlation coefficient ρ (equation (15)) increases with each correction step. In addition, as figure 4 clearly shows, both small and large displacements are estimated with equal SNR_e due to the inherent precision of the tracking method.

Once decoupling has occurred, the second elevational and third axial and lateral displacements are used to estimate the three shear strain components (equation (2), figure 6). Therefore, mapping of the full strain tensor (equation (1)) in that plane is achieved. The shear strain elastograms are noisier than the normal strain elastograms (figure 5) for two reasons. First, the shear strain calculation involves two gradient operations and, therefore, double the noise of estimation, and second, the true shear strain (e.g. figure 6(*a*)) is smaller than the corresponding true normal strain (e.g. figure 5(*a*)) and, therefore, tests the precision of the estimator to a higher degree. In order to smooth the shear strain elastograms, we used a median filtering with a 5×5 mask.

4.2. 2D array example

A 2D array (60×60 A-lines) was used to estimate elevational motion in an elevational plane (figure 1), in the middle and along the axis of the cylindrical inclusion. So, unlike the 1.5D array example that only estimates the in-plane elevational strain, in this case we can also estimate the out-of-plane elevational strain, i.e. in a plane perpendicular to the axial plane (or, the plane of the 1.5D array). The same recorrelation method and parameters as in the previous example were used and the elevational tracking results are shown in figure 7. The true and

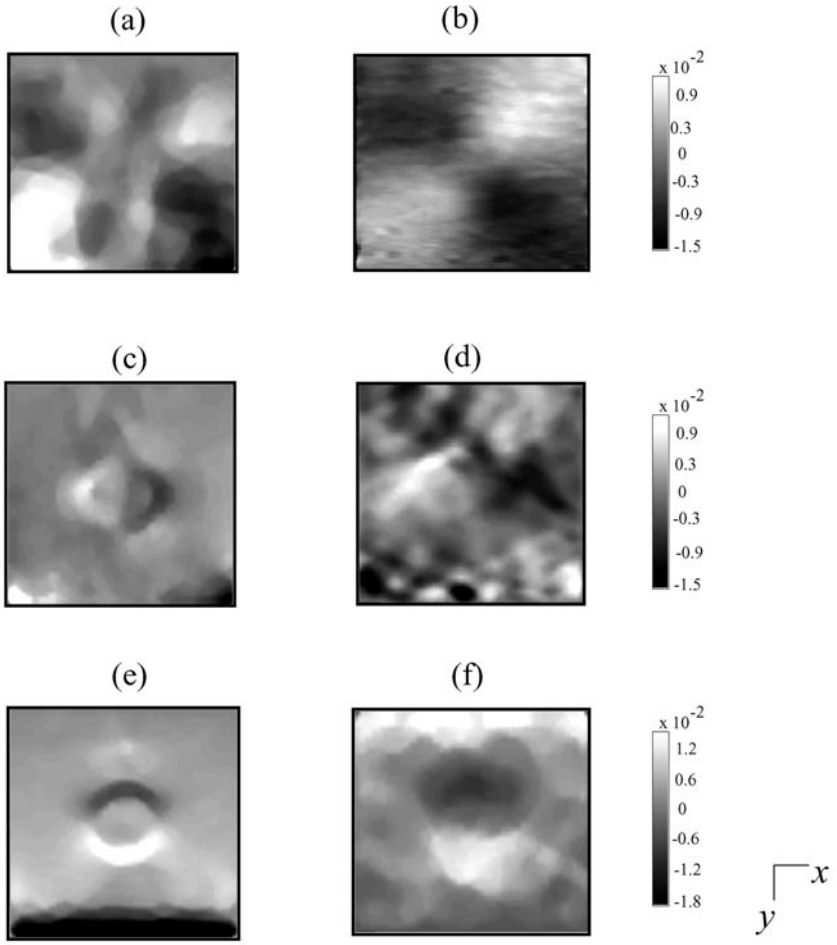

Figure 6. (*a*) True and (*b*) estimated shear elastogram (image of shear strain component ε_{xy}); (*c*) true and (*d*) estimated shear elastogram (image of shear strain component ε_{xz}); (*e*) true and (*f*) estimated shear elastogram (image of shear strain component ε_{xz}). Positive and negative strain values denote compressive and tensile strains respectively.

estimated elevational displacements are shown in figures 7(*a*) and 7(*c*) respectively. The true elevational displacement can also be observed on the left lateral side of its 3D equivalent in figure 3(*c*). Note that despite the skewed profile due to the non-slip conditions in that direction, the algorithm was able to estimate this complex linear motion (figure 7(*c*)). The cylindrical shape of the inclusion in the elevational direction is clearly shown in the elevational elastogram of figure 7(*d*), estimated using the least-squares estimator.

5. Discussion and conclusion

Using 3D FEA simulations we have shown that all three displacement vectors, and thereby principal normal as well as shear strain tensor components, can be estimated and imaged using a precision recorrelation method, using 1.5D or 2D arrays. Therefore, mapping and characterization of the full strain tensor (equation (1)) in a given plane was shown to be

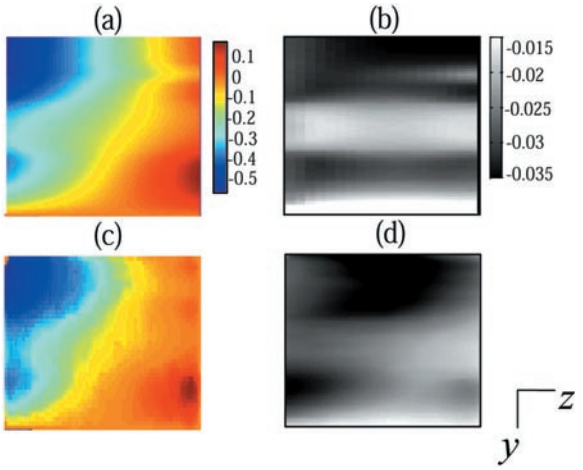

Figure 7. True elevational (*a*) displacement (in mm) and (*b*) strain, and estimated elevational (*c*) displacement (in mm) and (*d*) elastogram using a 2D array. Note the asymmetry of the displacement compared with figures 4(*a*) and 4(*d*) due to the imposed non-slip conditions in the elevational direction. Positive and negative strain values denote compressive and tensile strains respectively.

feasible. In the case of 2D arrays, precision estimations of elevational displacement and strain can be made at any plane perpendicular to the axial compression/scanning plane. These arrays are not currently available in our experimental setting and, therefore, these results have not been experimentally corroborated.

The wealth of information achieved with the 3D displacement field and strain tensor estimation may provide important insight into the fundamental mechanical properties of tissues, such as anisotropy, incompressibility, poroelasticity, viscoelasticity, lesion mobility and/or thermoelasticity. By measuring the Poisson's ratio through its definition as a ratio between orthogonal strains in all three dimensions, we can assess the anisotropy and incompressibility of the target (Konofagou and Ophir 1998). By definition, an incompressible material has a Poisson's ratio equal to 0.5. Also, if this parameter is measured versus time, e.g. during a stress relaxation experiment, the poroelastic properties of the tissue, i.e. the content of a fluid within the solid matrix, can be indicated, and the permeability as well as stiffness of the solid matrix can be quantified. In addition, the shear strain can be used to investigate the mobility of lesions within the target and thereby assess its type, i.e. malignant or benign (Chen 1995, Konofagou 1999). Finally, the undesired effect of changes in the speed of sound on thermal strain measurements in the axial direction can be compared with the measurement in the transverse directions, where the same effect is non-existent; this should allow the removal of this effect from the measurement of the thermal expansion coefficient in tissues.

Acknowledgments

This work was supported by National Cancer Institute Program Project Grant PO1-CA-64597. The authors would also like to thank Faouzi Kallel for his input in the 3D simulations.

References

Alam S K and Ophir J 1997 On the use of envelope and RF signal decorrelation as tissue strain estimators *Ultrasound Med. Biol.* **23** 1427–33

Bamber J C and Bush N L 1996 Freehand elasticity imaging using speckle decorrelation rate *Acoust. Imaging* **22** 285–92

Céspedes E I 1993 Elastography: imaging of biological tissue elasticity *PhD Dissertation* University of Houston, TX

Céspedes I and Ophir J 1993 Reduction of image noise in elastography *Ultrason. Imaging* **15** 89–102

Chaturvedi P, Insana M and Hall T 1998 2D companding for noise reduction in strain imaging *IEEE Trans Ultrason. Ferroelectr. Freq. Control* **45** 179–91

Chen E 1995 Ultrasound tissue displacement and tissue elasticity imaging *PhD Dissertation* University of Illinois, Urbana

Garra B S, Céspedes E I, Ophir J, Spratt R S, Zuurbier R A, Magnant C M and Pennanen M F 1997 Elastography of breast lesions: Initial clinical results *Radiology* **202** 79–86

Insana M, Chaturvedi P, Hall T and Bilgen M 1997 3D companding using 1.5D arrays for improved strain imaging *IEEE Ultrasonics Symp.* pp 1427–30

Insana M F, Wagner R F, Brown D G and Hall T J 1990 Describing small-scale structure in random media using pulse-echo ultrasound *J. Acoust. Soc. Am.* **87** 179–92

Insana M F, Wagner R F, Garra B S, Brown D G and Shawker T H 1986 Analysis of ultrasound image texture via generalized Rician statistics *Opt. Eng.* **25** 743–8

Kallel F and Ophir J 1997 Three dimensional tissue motion and its effects on image noise in elastography *IEEE Trans. Ultrason. Ferroelectr. Freq. Control* **44** 1286–96

Konofagou E E 1999 Estimation and imaging of three-dimensional motion and Poisson's ratio in elastography *PhD Dissertation* University of Houston, TX

Konofagou E E, Harrigan T, Ophir J and Krouskop T 1999 Poroelastography: estimating and imaging the poroelastic properties of tissues *IEEE Ultrasonics Symp.* at press

Konofagou E E and Ophir J 1998 A new method for estimation and imaging of lateral strains and Poisson's ratios in tissues *Ultrasound Med. Biol.* **24** 1183–99

Li W, Mastik F, Céspedes I, Carlier S and van der Steen A 1999 Echo decorrelation estimated from signal powers *Ultrasound Med. Biol.* **25** 405–9

Ophir J, Céspedes I, Ponnekanti H, Yazdi Y and Li X 1991 Elastography: a quantitative method for imaging the elasticity of biological tissues *Ultrasonic Imaging* **13** 111–34

Varghese T, Ophir J and Céspedes E I 1996 Noise reduction in elastography using temporal stretching with multicompression averaging *Ultrasound Med. Biol.* **22** 1042–53

Wagner R F, Smith S W, Sandrik J M and Lopez H 1983 Statistics of speckle in ultrasound B-scans *IEEE Trans. Sonics Ultrasonics* **30** 156–63